AGU PUBLICATIONS

JGR

Journal of Geophysical Research: Space Physics

RESEARCH ARTICLE
10.1002/2015JA021881

Key Points:
- Fermi 091214 event time histogram accurately reproduced
- The synthetic time histogram is reproducible by a wide range of possible TGFs
- The lepton time histogram can be split into three populations by looking at the pitch angles

Correspondence to:
D. Sarria,
david.sarria.89@gmail.com

Citation:
Sarria, D., P.-L. Blelly, M. S. Briggs, and F. Forme (2016), Studying the time histogram of a terrestrial electron beam detected from the opposite hemisphere of its associated TGF, *J. Geophys. Res. Space Physics*, *121*, 4698–4704, doi:10.1002/2015JA021881.

Received 4 SEP 2015
Accepted 23 MAR 2016
Accepted article online 28 MAR 2016
Published online 12 MAY 2016

Studying the time histogram of a terrestrial electron beam detected from the opposite hemisphere of its associated TGF

D. Sarria[1,2], P.-L. Blelly[1,2], M. S. Briggs[3,4], and F. Forme[1,2]

[1]Universite de Toulouse, UPS-OMP, IRAP, Toulouse, France, [2]CNRS, IRAP, Toulouse Cedex 4, France, [3]CSPAR, University of Alabama in Huntsville, Huntsville, Alabama, USA, [4]Department of Space Sciences, University of Alabama in Huntsville, Huntsville, Alabama, USA

Abstract Terrestrial gamma-ray flashes are bursts of X/gamma photons, correlated to thunderstorms. By interacting with the atmosphere, the photons produce a substantial number of electrons and positrons. Some of these reach a sufficiently high altitude that their interactions with the atmosphere become negligible, and they are then guided by geomagnetic field lines, forming a Terrestrial Electron Beam. On 9 December 2009, the Gamma-Ray Burst Monitor (GBM) instrument on board the Fermi Space Telescope made a particularly interesting measurement of such an event. To study this type of event in detail, we perform Monte-Carlo simulations and focus on the resulting time histograms. In agreement with previous work, we show that the histogram measured by Fermi GBM is reproducible from a simulation. We then show that the time histogram resulting from this simulation is only weakly dependent on the production altitude, duration, beaming angle, and spectral shape of the associated terrestrial gamma-ray flash. Finally, we show that the time histogram can be decomposed into three populations of leptons, coming from the opposite hemisphere, and mirroring back to the satellite with or without interacting with the atmosphere, and that these populations can be clearly distinguished by their pitch angles.

1. Introduction

The terrestrial gamma-ray flashes (TGFs) are bursts of X and gamma rays associated with lightning and detected mostly from space. TGFs were first presented by *Fishman et al.* [1994], using data from the BATSE experiment onboard NASA's CGRO spacecraft. A few years later, TGFs were detected from space by RHESSI [*Smith et al.*, 2005], AGILE [*Marisaldi et al.*, 2014], and Fermi Gamma-Ray Burst Monitor (GBM) [*Briggs et al.*, 2010]. Space experiments dedicated to the study of TGFs, such as ASIM (MXGS instrument) [*Neubert et al.*, 2006] and TARANIS (XGRE and IDEE instruments) [*Lefeuvre et al.*, 2009] are planned for the next years.

A comprehensive review of the high-energy emissions associated with lightning is presented in *Dwyer et al.* [2012]. The production mechanism of TGFs may be explained by the relativistic feedback discharge model [*Dwyer*, 2012] or the cold runaway mechanism [*Moss et al.*, 2006; *Celestin et al.*, 2012; *Chanrion et al.*, 2014]. Observations of TGFs from space, together with their associations with radio emissions from ground, allow constraining some important properties. TGFs consist of photons with a Bremsstrahlung type energy spectrum of about 30 MeV maximum energy, with a typical duration of 0.4 ms at satellite altitude [*Briggs et al.*, 2013] and their emission altitude should be located between 10 and 20 km [*Dwyer and Smith*, 2005; *Cummer et al.*, 2014]. They have a fluence of ~0.2 photon/cm^2 at satellite altitude [*Fitzpatrick et al.*, 2014], which requires $\gtrsim 10^{16}$ high-energy photons to be produced at the source.

Once produced, these primary photons from the TGF interact with the atmosphere. As a result of these interactions, secondary electrons and positrons are produced, and some of these particles can reach an altitude where they stop interacting significantly with the atmosphere. Their motion is then guided by the geomagnetic field, forming the so-called Terrestrial Electron Beams (TEBs) [*Dwyer et al.*, 2008]. Following field lines, TEB particles can travel from one hemisphere to the other and can lead to TGF detections that are actually due to electrons and positrons, like the anomalous RHESSI TGF event [*Smith et al.*, 2006] detected above a desert. Such events are significantly longer that TGFs, with a typical duration >1 ms. In some cases, due to the conservation of the first adiabatic invariant, some of the electrons can mirror and return to the

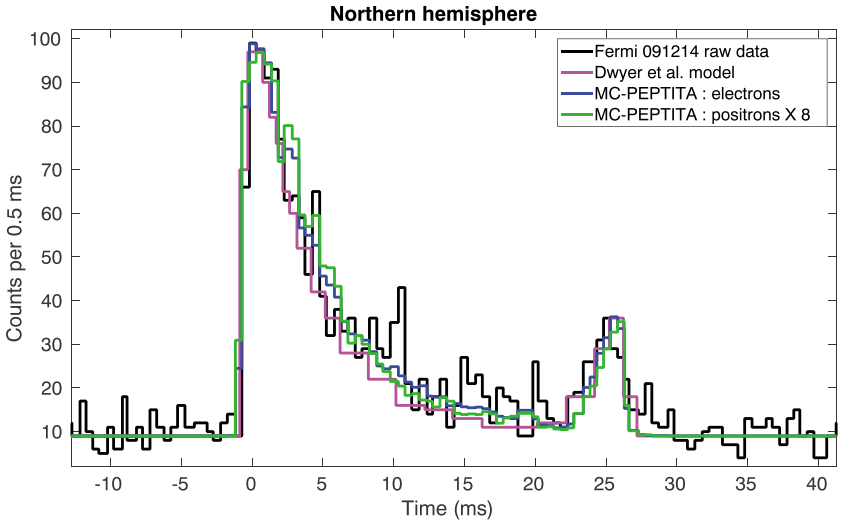

Figure 1. Time histogram of the Fermi 091214 event. Comparison between the data from Fermi GBM and the simulations of Dwyer et al. (both extracted from *Briggs et al.* [2011]) and our MC-PFEPTITA simulations (for electrons and positron). The counts for the positron histogram are multiplied by 8.

satellite, creating a specific signature of a dual pulse in the satellite measurement. Such events could be found in BATSE's data [*Dwyer et al.*, 2008] and later with Fermi GBM, particularly with the 091214 event [*Briggs et al.*, 2011]. This last event has a high-absolute brightness, making it a good candidate for simulations. During the 091214 event, Fermi was located at $\lambda = 25.34°$ latitude (N) and $\phi = 31.42°$ longitude (E). The light curve of this event, taken from *Briggs et al.* [2011], is displayed in Figure 1 (black curve). In this article, the likely source of the TGF responsible of the TEB ($\lambda \approx -13.0°$, $\phi \approx 32.0°$) has been determined by tracing back the geomagnetic field line from the observation location at ~565 km altitude.

For this study, we performed Monte-Carlo simulations, using the MC-PEPTITA model (Monte-Carlo Photon Electron Positron Tracking In Terrestrial Atmosphere), detailed in [*Sarria et al.*, 2015]. First, we discuss the initial conditions of the simulations and define a standard TGF case. Then we study how the synthetic TEB time histogram is sensitive to changes in the characteristics of the TGF (production altitude, duration, beaming angle, and spectral shape). Finally, we show how this time histogram can be decomposed by looking at the pitch angles of the leptons.

2. Initial Conditions

We take the estimation of *Briggs et al.* [2011] for the location of the source. For a TGF, a fluence of 0.2 photon/cm^2 at satellite altitude requires to have $\gtrsim 10^{16}$ produced in the source region. This quantity is not achievable in simulations in a reasonable amount of time. So a simulation is started with $N_p = 10^8$ photons, which ensures sufficient statistics to build the necessary distributions with low noise.

The altitude where the TGF's Bremsstrahlung photons are produced is set to $h = 15$ km for the standard case.

Following *Carlson et al.* [2011], the angle distribution has a normal distribution ($\propto \exp\left(-\theta^2/2\sigma_\theta^2\right)$) that has a σ_θ parameter, set to 35° for the standard case, consistent with *Carlson et al.* [2007], *Hazelton et al.* [2009], and *Gjesteland et al.* [2011]. The photon beam is assumed to be centered around the zenith.

Let E be the energy of a primary photon. We define a standard TGF spectrum with an energy distribution function $P(E) \propto 1/E \exp(-E/\epsilon)$, where ϵ is the cutoff energy with a value set to 7.3 MeV. This makes this spectrum reasonably close to the predicted spectrum [*Dwyer et al.*, 2012]. The threshold energy is set to 10 keV and the maximum energy to 30 MeV.

Fitzpatrick et al. [2014] indicates that Fermi observations are consistent with Gaussian TGF photons pulses at the source with a sigma parameter between 0.025 ms and 0.1 ms. Furthermore, the Relativistic Feedback Discharge Model (RFD) [*Dwyer*, 2012] gives time distributions of the primary photons that are roughly symmetrical for all pulse duration. Therefore, we also make the assumption that the temporal distribution

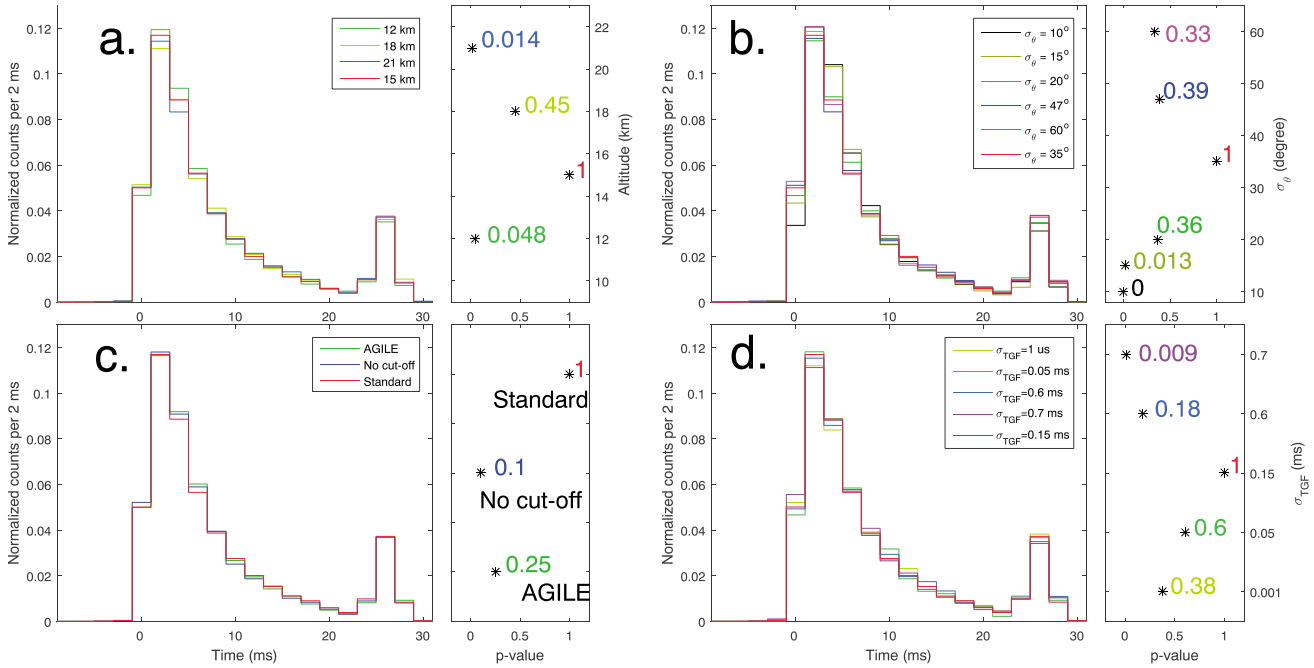

Figure 2. Simulated time histograms of the Fermi 091214 event, considering different changes on some parameters of the supposed TGF photon source: (a) altitude, (b) beaming angle, (c) energy spectrum, and (d) time distribution. For each case, *p* values are given, that indicates the level of similarities between the simulated data sets, with respect to the standard case (always displayed in red).

the TGF pulse follows, at the source, a Gaussian distribution, with a sigma parameter noted σ_{TGF}. A value of $\sigma_{TGF} = 0.15$ ms is used for the standard case.

In the simulations, the status (energy, position, and velocity) of each lepton is saved when it crosses 565 km altitude (close to Fermi location), downward or upward. All the lepton distributions that are discussed hereafter are built considering only the particles in the Northern Hemisphere, with a radial distance lower than 50 km from the center of the beam. This distance is chosen to cover 90% of the lepton beam [*Sarria et al.*, 2015].

3. Basic Comparison

Figure 1 shows the time distribution of the electrons and positrons reaching the satellite altitude in the Northern Hemisphere. We compare the simulated data (blue curve for electrons and green curve for positrons) with the measurement made by Fermi GBM.

A simple model using three parameters (a time shift $t_s = -19.2$ ms, a scale factor $A = 1/62.9$, and a constant background rate $b = 9$ counts per 0.5 ms) is applied to the simulated time histograms to match the Fermi histogram. The two histograms fit accurately, with a coefficient of determination $r^2 = 0.92$. This is similar to the result of the simulation done by Dwyer et al., that is also presented in [*Briggs et al.*, 2011], and reproduced in Figure 1 (magenta curve). This confirms independently that this time histogram is due to leptons that are coming to the satellite from the Southern Hemisphere (for the first pulse between 0 ms and 12 ms), with a part that is then bouncing on a magnetic mirror point and reaching the satellite a second time (for the second pulse between 21 and 27 ms). The positron histogram is very similar to the electron histogram, but with a scale factor in the number of counts of $A_p = 8$.

Nevertheless, care should be taken with such a comparison, since the histogram for the Fermi GBM data shows the detected counts not corrected for the detection response to the incident flux, whereas simulations give the physical flux of leptons. This should not significantly change this basic comparison, but it should be taken into account for a more precise comparison between satellite data and simulations.

In the next section, we explore what are the possible ranges of parameters of the TGF that still give time histograms similar to the simulation described in this section, with the baseline standard parameters.

4. Effects of Different TGF Sources

Figure 2 shows the time histogram made from the leptons reaching satellite altitude in the Northern Hemisphere but with variations of some parameters from the standard TGF described in section 2. The lepton time histogram is built by summing electrons and positrons. The time bin widths are increased to 2 ms, to reduce the statistical noise. The data constituting each time histogram, each resulting from a simulation with a change of parameter, are compared with a baseline simulation resulting from the standard parameters. For this comparison, we use a two-sample Kolmogorov-Smirnov test [*Pearson et al.*, 1954], that permits calculating a corresponding p value, with a significance level set to 5%. The assumed null hypothesis of this test is that the data making the two time histograms that are compared come from the same continuous distribution, i.e., the effect of the change of a given parameter cannot be observed. A p value lower than 0.05 means that this null hypothesis should be rejected. A p value greater than 0.1 indicates that the null hypothesis has no reason to be rejected. A p value of 1 is obtained if we compare the same two data sets.

In Figure 2a, the altitude where the TGF's photons are produced is tested at 12, 18, and 21 km. A source at 12 km altitude gives a p value of 0.048, which is slightly under the rejection threshold. Photon productions altitudes set to 18 km and 21 km give p values of 0.444 and 0.014, respectively. Therefore, the statistical test indicates that by using only the time distributions of these simulations, source altitudes between 12 and 18 km cannot be significantly distinguished from an altitude of 15 km, but a source at 21 km or below 12 km produces a time distribution that is significantly different from that of the standard altitude of 15 km. It is worth mentioning that the current understanding about TGFs seems to favor sources altitudes below 15 km [*Cummer et al.*, 2014].

In Figure 2b, the σ_θ parameter of the beaming angle of the TGF photon source is varied to 10°, 15°, 20°, 35°, 47°, and 60°. Values of σ_θ between 20° and 60° give p values well above 0.1; thus, they do not result in significant changes in the time histogram. A source with $\sigma_\theta = 15°$ or less gives p values below 0.05. Therefore, TGF sources with half opening angles between ≈20° and 60° are not distinguishable by looking only to this electron time histogram.

In Figure 2c, the energy spectrum of the photon source is changed. The standard case is described in section 2. The AGILE case uses an initial photon source that results in a photon spectrum, at satellite altitude, that approximately corresponds to the cumulative spectrum seen in the AGILE data [*Tavani et al.*, 2011]. One can use a broken power law with powers $I_1 = -1, I_2 = -3$, a break at 7.1 MeV and energies up to 100 MeV. The "no cutoff" case uses a simple $\propto 1/E$ energy spectrum with energies up to 30 MeV. For the two cases, the null hypothesis is never rejected, since the corresponding p values are greater than 0.1. Therefore, the TEB time histogram is very weakly dependent on the spectral shape of the initial TGF.

The time histograms of Figure 2d result from initial photon sources with values of σ_{TGF} of 1 μs, 0.05 ms, 0.15 ms, 0.6 ms, and 0.7 ms. Compared to the standard case (where $\sigma_{TGF} = 0.15$ ms) the statistical test gives p values greater than 0.1 for σ_{TGF} less than 0.6 ms. Using a TGF arbitrarily shorter than a few μs would lead to the same result. Actually the scale of time delays and scatterings of the TEB leptons that are traveling though the atmosphere and then along the magnetic field lines (all with a different status once escaping the atmosphere) are of the order of 10−20 ms, which is much larger than these values of σ_{TGF}. If the TGF is longer, with $\sigma_{TGF} > 0.7$ ms, the test indicates a significant difference with the standard case (p value <0.05).

5. Pitch Angle Decomposition

Let v be the magnitude of the velocity vector of a lepton, which is constant when the lepton is not interacting with the atmosphere, because of energy conservation. Let $v_{\parallel}$ be the component of the velocity vector that is parallel to its local geomagnetic field. The pitch angle α of a lepton is defined as the angle between its velocity vector and the local magnetic field direction vector. Figures 3a and 3b show the time distribution of leptons crossing satellite altitude in the Northern Hemisphere. In the following, we use the same definitions of the normal and lognormal distributions that are presented in [*Briggs et al.*, 2010], as well as a Poisson log-likelihood minimization to find the best fits.

Figure 3a shows the time distribution of the leptons that are coming from the Southern Hemisphere and is equivalent to having pitch angles α between 0° and 90°. The time distribution of the leptons of Figure 3a can be very well fit with a lognormal distribution (red curve). This fit gives a coefficient of determination $r^2 = 0.99$. This lognormal time distribution is due to differences in pitch angles α of the leptons when they escape the atmosphere. Actually, all the leptons will follow very similar magnetic field lines, but the ones with the lowest

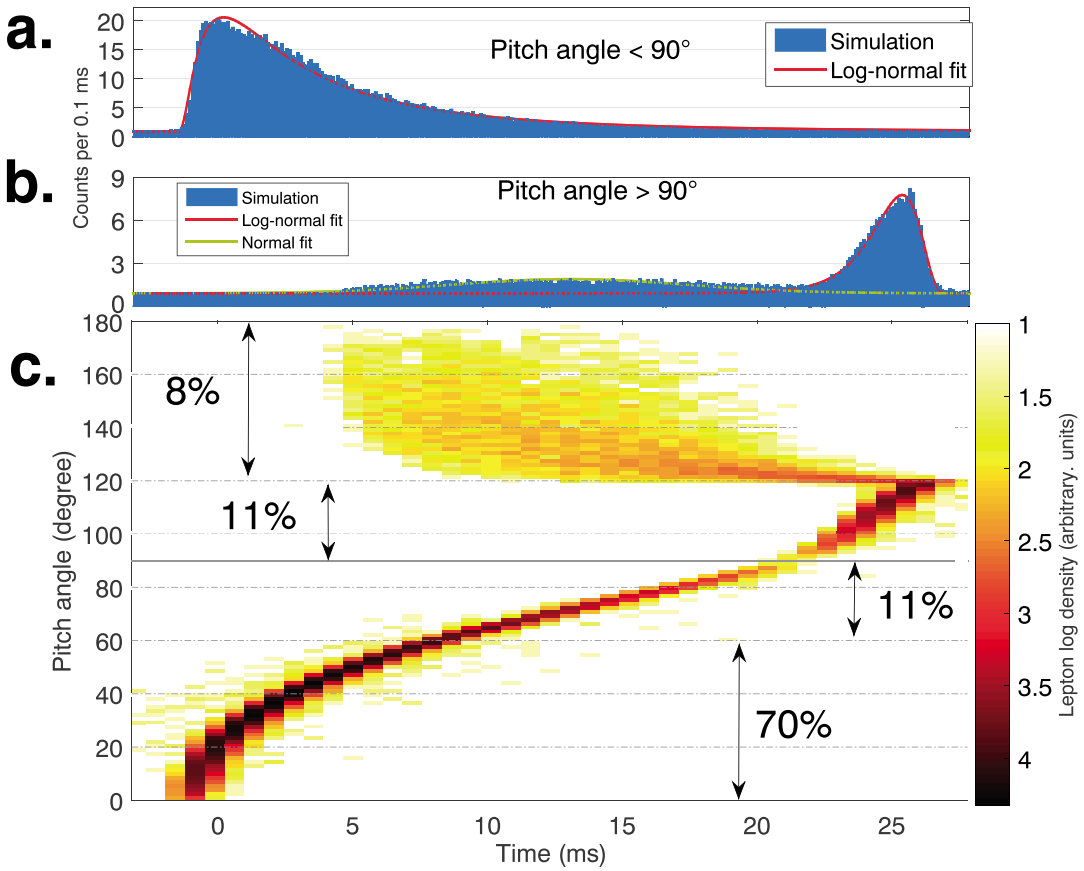

Figure 3. Time and pitch angles distributions for leptons in the Northern Hemisphere, crossing the altitude of the satellite. The time scale (*x* axis) is shared by the three subfigures. Leptons coming to the satellite from the Southern Hemisphere will have a pitch angle between 0° and 90°, whereas leptons coming back after mirroring will have pitch angles between 90° and 180°. (a) Simulated time history, only for leptons with pitch angles <90°. The red curve is a lognormal fit. (b) Simulated time history, only for leptons with pitch angles >90°. The red curve is a lognormal fit, and the black curve is a normal fit. (c) Density distribution of pitch angle versus time. The fractions of the total number of leptons included inside some pitch angle ranges are given.

starting pitch angles will have the highest $v_{\|}$ (still in the case where $\alpha < 90°$). The two quantities are linked via $v_{\|} = v\ \cos(\alpha)$ and α increases along the trajectory of the lepton, in order to conserve the first adiabatic invariant. At satellite altitude, the average value of v is ≈0.98 c and the average value of $v_{\|}$ is ≈0.5 c.

The time distribution of Figure 3b can be split into two contributions. From about 5 to 21 ms, we see that the distribution can be very well fit using a normal distribution. The population located from about 21 to 27 ms (also called "the second pulse") can be well fit by a mirrored lognormal distribution. This model fits very well the data since its overall coefficient of determination is $r^2 = 0.98$. These two subpopulations of leptons can be easily separated with their pitch angles, as shown by Figure 3c. There is a clear difference between the leptons above and below $\alpha \approx 120°$. Actually, a pitch angle of about 120° at this position ($h = 565$ km, $\lambda = 25.5°$, and $\phi = 31.4°$) corresponds to electrons that had a mirroring altitude of about 100 km, the altitude above which the interactions with the atmosphere occur so infrequently that they become negligible. Therefore, we define 100 km as the limit of the atmosphere in this context. Below ≈120°, the distribution is weakly spread and corresponds to the leptons that had a pitch angle between ≈60° and 90° and came back to satellite altitude after mirroring, without interacting significantly with the atmosphere. Indeed, Figure 3c shows that the number of leptons between 60° and 90° is similar to the number between 90 and ≈120°, each representing ≈11% of the total count. All the leptons that are coming to the satellite with pitch angles below ≈60° were inside the loss cone (the range of angles where the particles have mirroring altitudes inside the atmosphere), but not all of them are lost. A portion (≈8% of the total count) can mirror back to satellite altitude. These leptons interacted weakly enough with the atmosphere (otherwise they would have lost too much energy and have fallen below the threshold energy of 10 keV) but strongly enough to be

scattered back outside the atmosphere. Random interactions with the atmosphere result in random time delays, so that the overall resulting time distribution of this population, seen at satellite altitude, has approximately a normal shape.

6. Conclusions

We performed MC-PEPTITA simulations of a TGF/TEB event, in a configuration very similar to Fermi 091214 event. A reasonable standard TGF was defined with relevant parameters for its position, energy spectrum, beaming, and time distribution. The standard parameters for the simulation produce a time history very similar to the Fermi observation. Additionally, we show that the simulated TEB time histograms are weakly sensitive to the altitude and opening angles of the leptons, and virtually insensitive to the spectrum and duration. Indeed, these sets of parameters produce very similar time profiles :

1. Standard or AGILE type energy spectra.
2. Photon source altitudes ranging from 12 to 18 km.
3. Beaming angles from $\sigma_\theta = 20°$ to $\sigma_\theta = 60°$.
4. TGF photon time pulses with σ_{TGF} arbitrarily small, up to about 0.6–0.7 ms.

In configuration similar to the 091214 event, we think that the time histogram is mostly influenced by two factors : the shape of the geomagnetic field that is guiding the leptons and their pitch angle distribution once they escape the atmosphere. This second factor may be strongly influenced by the tilt angle of the TGF; it will be studied in a forthcoming work.

Finally, we showed that this TEB time histogram can be decomposed into three populations. The first population, coming directly from the hemisphere where the TGF was originally emitted, has pitch angles between 0° and 90° and has a lognormal time distribution. The leptons that are going back to the satellite altitude after mirroring have pitch angles between 90° and 180° and can be decomposed into two population : the leptons that have significantly interacted with the atmosphere and the leptons that did not. If they interacted, their pitch angles are between ≈120° and 180°, and their lightcurve can be well represented by a normal distribution. If they did not, their pitch angles are between 90° and ≈120° and their time distribution can be well represented with a mirrored lognormal distribution.

The TARANIS satellite, with the IDEE instrument, will have the ability to measure the pitch angle distribution of the electrons and should provide reliable information about these properties.

Fermi GBM also measured the associated energy spectrum, which made it possible to estimate the positron fraction of the TEB [*Briggs et al.*, 2011]. These two features may be used to better determine the allowed ranges of properties of the TGF that produced this TEB, a study that we will perform in a future work.

Acknowledgments
We want to thank the two anonymous reviewers for their recommendations and comments that helped to greatly improve this work. We would like to thank the CNES (Centre National d'Etudes Spatiales) and the DGA (Direction Generale de l'Armement) for their financial support. This work was granted access to the HPC resources of CALMIP supercomputing center under the allocation 2015-p1505. The data generated by the MC-PEPTITA simulations presented in this work can be requested by emailing the corresponding author: david.sarria.89@gmail.com.

References

Briggs, M. S., et al. (2010), First results on terrestrial gamma ray flashes from the Fermi Gamma-ray Burst Monitor, *J. Geophys. Res.*, *115*, A07323, doi:10.1029/2009JA015242.

Briggs, M. S., et al. (2011), Electron-positron beams from terrestrial lightning observed with Fermi GBM, *Geophys. Res. Lett.*, *38*, L02808, doi:10.1029/2010GL046259.

Briggs, M. S., et al. (2013), Terrestrial gamma-ray flashes in the Fermi era: Improved observations and analysis methods, *J. Geophys. Res. Space Physics*, *118*, 3805–3830, doi:10.1002/jgra.50205.

Carlson, B. E., N. G. Lehtinen, and U. S. Inan (2007), Constraints on terrestrial gamma ray flash production from satellite observation, *Geophys. Res. Lett.*, *34*, L08809, doi:10.1029/2006GL029229.

Carlson, B. E., T. Gjesteland, and N. Østgaard (2011), Terrestrial gamma-ray flash electron beam geometry, fluence, and detection frequency, *J. Geophys. Res.*, *116*, A11217, doi:10.1029/2011JA016812.

Celestin, S., W. Xu, and V. P. Pasko (2012), Terrestrial gamma ray flashes with energies up to 100 MeV produced by nonequilibrium acceleration of electrons in lightning, *J. Geophys. Res.*, *117*, A05315, doi:10.1029/2012JA017535.

Chanrion, O., Z. Bonaventura, D. Çinar, A. Bourdon, and T. Neubert (2014), Runaway electrons from a "beam-bulk" model of streamer: Application to TGFs, *Environ. Res. Lett.*, *9*(5), 055003, doi:10.1088/1748-9326/9/5/055003.

Cummer, S. A., M. S. Briggs, J. R. Dwyer, S. Xiong, V. Connaughton, G. J. Fishman, G. Lu, F. Lyu, and R. Solanki (2014), The source altitude, electric current, and intrinsic brightness of terrestrial gamma ray flashes, *Geophys. Res. Lett.*, *41*, 8586–8593, doi:10.1002/2014GL062196.

Dwyer, J. R. (2012), The relativistic feedback discharge model of terrestrial gamma ray flashes, *J. Geophys. Res.*, *117*, A02308, doi:10.1029/2011JA017160.

Dwyer, J. R., and D. M. Smith (2005), A comparison between Monte Carlo simulations of runaway breakdown and terrestrial gamma-ray flash observations, *Geophys. Res. Lett.*, *32*, L22804, doi:10.1029/2005GL023848.

Dwyer, J. R., B. W. Grefenstette, and D. M. Smith (2008), High-energy electron beams launched into space by thunderstorms, *Geophys. Res. Lett.*, *35*, L02815, doi:10.1029/2007GL032430.

Dwyer, J. R., D. M. Smith, and S. A. Cummer (2012), High-energy atmospheric physics: Terrestrial gamma-ray flashes and related phenomena, *Space Sci. Rev.*, *173*, 133–196, doi:10.1007/s11214-012-9894-0.

Fishman, G. J., et al. (1994), Discovery of intense gamma-ray flashes of atmospheric origin, *Science*, *264*, 1313–1316, doi:10.1126/science.264.5163.1313.

Fitzpatrick, G., et al. (2014), Compton scattering in terrestrial gamma-ray flashes detected with the Fermi gamma-ray burst monitor, *Phys. Rev. D*, *90*(4), 043008, doi:10.1103/PhysRevD.90.043008.

Gjesteland, T., N. Østgaard, A. B. Collier, B. E. Carlson, M. B. Cohen, and N. G. Lehtinen (2011), Confining the angular distribution of terrestrial gamma ray flash emission, *J. Geophys. Res.*, *116*, A11313, doi:10.1029/2011JA016716.

Hazelton, B. J., B. W. Grefenstette, D. M. Smith, J. R. Dwyer, X.-M. Shao, S. A. Cummer, T. Chronis, E. H. Lay, and R. H. Holzworth (2009), Spectral dependence of terrestrial gamma-ray flashes on source distance, *Geophys. Res. Lett.*, *36*, L01108, doi:10.1029/2008GL035906.

Lefeuvre, F., E. Blanc, and J. L. Pinçon (2009), TARANIS—A satellite project dedicated to the physics of TLEs and TGFs, *AIP Conf. Proc.*, *1118*, 3–7, doi:10.1063/1.3137711.

Marisaldi, M., et al. (2014), The first AGILE low-energy (<30 MeV) Terrestrial Gamma-ray Flashes catalog, Geophysical Research Abstracts vol.16, EGU2014-11326-1 presented at 2014 EGU General Assembly Conference, Vienna, Austria, 27 April–2 May.

Moss, G. D., V. P. Pasko, N. Liu, and G. Veronis (2006), Monte Carlo model for analysis of thermal runaway electrons in streamer tips in transient luminous events and streamer zones of lightning leaders, *J. Geophys. Res.*, *111*, A02307, doi:10.1029/2005JA011350.

Neubert, T., I. Kuvvetli, C. Budtz-Jørgensen, N. Østgaard, V. Reglero, and N. Arnold (2006), The atmosphere-space interactions monitor (ASIM) for the international space station, in *Proceedings of the ILWS Workshop, Goa, India, 19–24 Feb.*, edited by N. Gopalswamy and A. Bhattacharyya, p. 448.

Pearson, E. S., K. Pearson, and H. O. Hartley (1954), *Biometrika Tables for Statisticians*, Univ. Press, Cambridge, U. K.

Sarria, D., P.-L. Blelly, and F. Forme (2015), MC-PEPTITA: A Monte Carlo model for Photon, Electron and Positron Tracking in Terrestrial Atmosphere–Application for a terrestrial gamma-ray flash, *J. Geophys. Res. Space Physics*, *120*, 3970–3986, doi:10.1002/2014JA020695.

Smith, D. M., L. I. Lopez, R. P. Lin, and C. P. Barrington-Leigh (2005), Terrestrial gamma-ray flashes observed up to 20 MeV, *Science*, *307*, 1085–1088, doi:10.1126/science.1107466.

Smith, D. M., et al. (2006), The anomalous terrestrial gamma-ray flash of 17 January 2004, *Eos Trans. AGU*, *87*(52), Fall Meet. Suppl., Abstract AE31A–1040.

Tavani, M., et al. (2011), Terrestrial gamma-ray flashes as powerful particle accelerators, *Phys. Rev. Lett.*, *106*, 018501, doi:10.1103/PhysRevLett.106.018501.